Article

NPP and Vegetation Carbon Sink Capacity Estimation of Urban Green Space Using the Optimized CASA Model: A Case Study of Five Chinese Cities

Fang Xu, Xiangrong Wang and Liang Li *

School of Landscape Architecture, Beijing Forestry University, Beijing 100083, China;
fangxu2019@bjfu.edu.cn (F.X.); xrw@bjfu.edu.cn (X.W.)
* Correspondence: liliang@bjfu.edu.cn

Abstract: Urban area is a major source of CO_2 and other greenhouse gases. Urban green space (UGS) is an essential element to increase carbon sequestration directly and reduce emission indirectly. In this study, the net primary production (NPP) and net ecosystem productivity (NEP) was monitored in order to enhance the carbon sequestration function of UGS and promote urban low-carbon development. Based on the Sentinel-2 L2A satellite images, meteorological data, and vegetation type data in 2019, we used the optimized Carnegie Ames Stanford Approach (CASA) model to estimate the NPP values of UGS types including attached green space, park green space, protective green space, and regional space in Beijing, Guangzhou, Shanghai, Shenyang, and Xi'an. The NEP values were evaluated based on NPP and soil heterotrophic respiration (R_H) to quantify the vegetation carbon sink capacity. The accuracy test shows that the estimated NPP values based on the optimized CASA model are effective. The results indicate that the average NPP values (1008.5 $gC \cdot m^{-2} \cdot a^{-1}$) and vegetation carbon sink capacity (771.49 $gC \cdot m^{-2} \cdot a^{-1}$) of UGS in Beijing rank first among the cities, which is followed by the values in Guangzhou. The regional green space and park green space in five cities function as carbon sinks with high NPP values and have vegetation carbon sink capacity, whereas the attached green space in Shanghai and Xi'an as well as the protective green space in Guangzhou and Xi'an function as carbon sources. Moreover, the NEP distribution shows obvious spatial aggregation characteristics, that is, the high NEP values of UGS are clustered in mountainous forest areas in the west and north of Beijing, Northeast Guangzhou, and South Xi'an whereas the low NEP values are mostly concentrated in the urban built-up areas under strong influences of human activities. This research provides a new method for NPP and NEP estimation of UGS at the city scale and the scientific basis for the improvement of the vegetation carbon sink capacity of UGS.

Keywords: light energy utilization; net primary productivity; net ecosystem productivity; urban green space; China

1. Introduction

A high density of the population is concentrated in urban areas and strong human activities influence the carbon cycle and emit large amounts of CO_2. Covering 2% of the global land, urban areas are responsible for approximately 75% of global carbon emission [1]. With rapid urbanization and industrialization, carbon emission in Chinese cities deserves special attention [2]. It is possible to remove atmospheric CO_2 by sequestering it in urban green space (UGS), which is one of the natural elements in urban areas [3]. Although the vegetation density in UGS is relatively smaller than in forests, it can be an essential carbon sink and the capacity was estimated in various cities [4]. It is challenging to measure carbon fluxes directly using eddy covariance measurements in cities [5]. Net ecosystem productivity (NEP) is an important indicator to describe the terrestrial ecosystem carbon cycle [6] which can be obtained by subtracting the soil heterotrophic respiration (R_H) from the net primary production (NPP) [7].

NPP is the total amount of organic matter accumulated by plants through photosynthesis conversion. It is an essential variable to characterize plant activities and can accurately reflect vegetation growth status [8]. Quantitative evaluation methods of NPP include field measurement and model estimation. Due to many constraints, it is usually difficult to realize field measurements of NPP in large-scale areas. However, remote sensing technology has advantages such as a short time span, wide coverage, low cost, and relative stability, therefore, most researchers use the model simulation method based on remote sensing to estimate NPP on a large scale [9]. The commonly used models for NPP estimation include the climate-related statistical models (e.g., Miami [10], Thornthwaite Memorial [11], and Chikugo [12]), ecosystem process model (e.g., BIOME-BGC [13]), and light energy utilization model (e.g., CASA [14]). The climate-related models were mainly used in the early stage of vegetation NPP studies. Such models are relatively simple and the required meteorological data are easy to obtain, which reflects potential vegetation NPP. Zhou et al. [15] studied the spatiotemporal variation of NPP in Tibet based on the Miami model and the Thornthwaite Memorial model. The ecosystem process models consider various factors such as plant photosynthesis, respiration, decomposition, and synthesis of organic matter. However, these models are relatively complex and the input data are difficult to obtain [16]. The CASA model is a representative model based on light energy utilization which has been used in a large number of studies at large scales ranging from worldwide to cities. Zhang et al. [17] studied the spatiotemporal dynamics and driving factors of NPP in Central Asia based on the CASA model and the Miami model. Zhou et al. [18] used the CASA model to simulate the total NPP of grassland in China during 1982–2010 which was 988.3 TgC and more than 60% of grassland showed an increasing trend. Peng et al. [19] used the CASA model to estimate NPP in Beijing and analyzed NPP responses to stages of urbanization. Among these models, the CASA model comprehensively considers the influences of different natural factors on vegetation NPP and its driving variable data are mostly derived from large-scale remote sensing images [20].

Besides the absorbed photosynthetically active radiation (APAR), the light utilization efficiency (LUE) is the main component of the CASA model [21]. Therefore, accurate estimation of LUE directly affects the NPP estimation accuracy [22]. As a necessary parameter for the calculation of LUE, the maximum LUE (ε_{max}) has a great influence on the estimation results of vegetation NPP. However, in the original CASA model, the maximum LUE (ε_{max}) value was uniformly set as 0.389 gC·MJ^{-1} [23]. However, this value varies with different vegetation types [24].

Moreover, the spatial resolution of current global NPP products ranges from 300 m to 5 km. For example, the MOD17A3HGF NPP product has a temporal resolution of 1 a and a spatial resolution of 500 m, which is relatively rough in certain regions and neglects the heterogeneity on a small scale. To support NPP and NEP estimation in cities with complex vegetation conditions and reduce uncertainty in terrestrial energy and carbon budgets, a dataset with higher spatial resolution is urgently required [25]. Unlike the 1 km AVHRR [26], the 500 m MODIS [27] and 30 m Landsat [28], Sentinel-2 satellite, which was launched on 23 June 2015, has a revisit period of ten days and a width of 290 km. Besides the characteristics of short revisit periods and rich band information, it has special advantages in vegetation information extraction because of its multiple narrow bands in the visible and near-infrared ranges [29].

In this study, we improved the CASA model by specifying ε_{max} values based on high-resolution satellite images to improve the NPP and NEP estimation accuracy of UGS in five representative cities in China including Beijing, Guangzhou, Shanghai, Shenyang, and Xi'an. This study aims to explore the spatial distribution pattern of vegetation NPP and NEP in UGS in Chinese cities and to compare the vegetation carbon sink capacity of different UGS types.

2. Materials and Methods

2.1. Study Area

In this study, five representative cities including Beijing, Guangzhou, Shanghai, Shenyang, and Xi'an were selected as study areas. These cities are distributed in different regions and they are experiencing rapid urbanization with increasing energy consumption and carbon emissions (Figure 1).
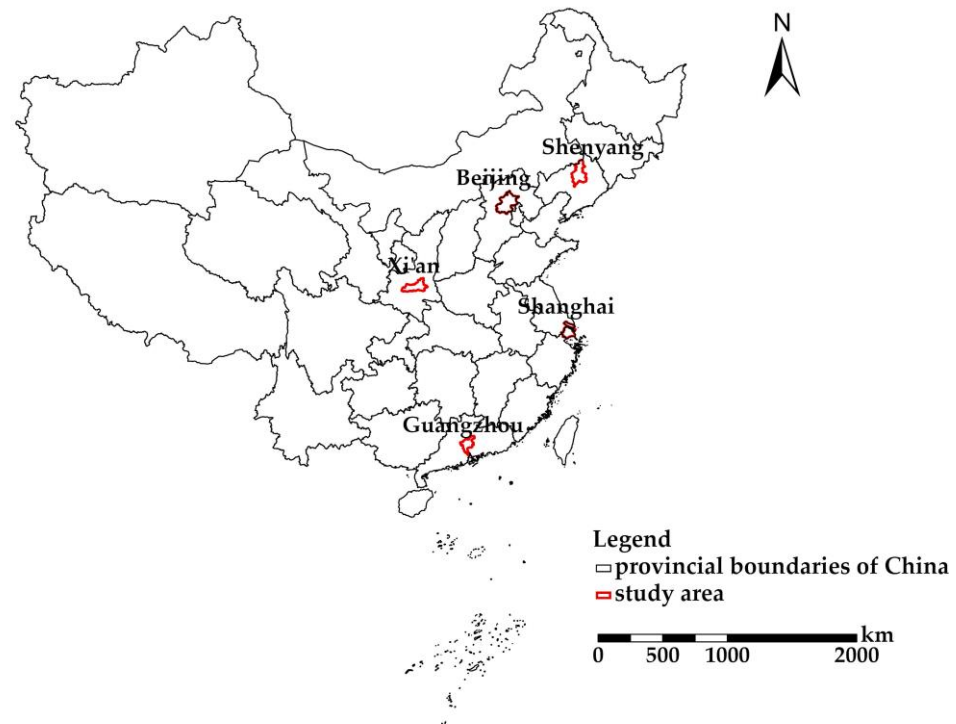
Figure 1. Geographical location of the study area.

Beijing (115°25′–117°35′ E, 39°28′–41°05′ N) is surrounded by mountains on three sides, with the terrain characteristics of high in the northwest and low in the southeast. The total area of Beijing is 16,410.54 km^2. It is in a warm temperate zone with a semi-humid and semi-arid monsoon climate. The annual average temperature is 12.9 °C and the annual average precipitation is 595 mm [30]. The forest coverage in Beijing reached 44.8% in 2022 [31].

Located in the Pearl River Delta, Guangzhou (112°57′–114°3′ E, 22°26′–23°56′ N) is adjacent to the Nanling Mountains in the north and the South China Sea in the south. The total administrative area of Guangzhou is 7434.40 km^2 with 11 districts. It has a marine subtropical monsoon climate with an average annual temperature of 21.7–23.1 °C and an average annual precipitation of 1923 mm. The terrain slopes from the northeast to the southwest with mountainous area in the northeast, a hilly basin in the middle, and the coastal alluvial plain in the south. The zonal vegetation is the south tropical monsoon evergreen broad-leaved forest, most of which are secondary forests and artificial forests [32].

Shanghai (120°51′–122°12′ E, 30°40′–31°53′ N) is located on the west coast of the Pacific Ocean, along the east coast of the Asian mainland, and is a part of the Yangtze River Delta alluvial plain. Shanghai has an administrative area of 6340.5 km^2 with 16 districts. Shanghai belongs to the north subtropical monsoon climate with short spring and autumn and long winter and summer. The city's average annual temperature is 17.9 °C and the average annual precipitation is 1474.5 mm [33].

Shenyang (123°18′–123°48′ E, 41°36′–41°57′ N) is located in the south of Northeast China, covering an area of 12,860 km^2. There are 13 county-level administrative districts in Shenyang. It has a temperate sub-humid continental climate with an average annual temperature of 8.5 °C and annual precipitation of 716 mm [34]. Shenyang is dominated by

plain terrain with an average elevation of about 50 m. Mountains and hills are concentrated in the northeast and southeast and are an extension of the Liaodong Hills. The western part of Shenyang belongs to the alluvial plain of the Liao River and the Hun River. The green space area with the urban built-up area covers 229.68 km^2, with a green space ratio of 40.08% [35].

Xi'an (107°24′–109°29′ E, 33°25′–34°27′ N) is located in Guanzhong Plain in the middle of the Yellow River Basin, covering an area of 10,108 km^2 with 11 districts and 2 counties. It is under a warm, temperate, sub-humid, and continental monsoon climate. The annual average temperature lies between 13.1 and 14.3 °C and the annual precipitation is between 528.3 and 716.5 mm. The average elevation of Xi'an is 400 m above sea level; however, it has the largest altitude difference among Chinese cities because it includes the Qinling Mountain and Weihe Plain [36].

2.2. Data Sources and Processing

2.2.1. Vegetation Type Data

Vegetation type data were obtained from the Global 30 m Fine Land Cover Product (GLC_FCS30_2019), which was downloaded from the Big Earth Data Science Engineering Program (https://data.casearth.cn/, accessed on 1 September 2020). According to this map, vegetation types in the study area include evergreen needle leaf forests, evergreen broad leaf forests, deciduous needle leaf forests, deciduous broad leaf forests, mixed forests, shrubland, grassland, cropland, and wetland.

2.2.2. NDVI

The normalized difference vegetation index (NDVI) was calculated by band operation based on the Sentinel-2 L2A satellite images in 2019, which were obtained from the Copernicus Data Access Center (https://scihub.copernicus.eu/dhus/#/home, accessed on 10 September 2020). The original images were processed by cutting, stitching, radiometric calibration, and atmospheric correction to obtain preprocessed images. Then, the monthly NDVI data were synthesized through the maximal value composite (MVC) method.

2.2.3. Meteorological Data

The meteorological data required for inputting the improved CASA model were obtained from the Dataset of Daily Values of Surface Climatological Data for China (V3.0) (http://data.cma.cn, accessed on 15 September 2020) provided by the National Meteorological Science Data Center of China. We calculated the monthly values of temperature, precipitation, evapotranspiration, and sunshine hours of 699 basic weather stations in 2019 based on this dataset. Then, the meteorological values of each city were obtained by spatial interpolation and clipping. In addition, solar radiation was simulated using the Angstrom–Prescott formula [37]:

$$R_t = (a + b\frac{n}{N})R_a \tag{1}$$

where N represents the maximum sunshine hours, n is the mean sunshine hours, R_t stands for the total solar radiation, and R_a represents the extraterrestrial radiation for the initial value. In this study, the coefficients a and b were set to 0.25 and 0.5 according to the Food and Agriculture Organization (FAO) recommended values.

2.2.4. MODIS NPP Product (MOD17A3H Version 6 Product)

The MODIS NPP values in 2019 with a spatial resolution of 500 m were derived from the MOD17A3H Version 6 product, which was downloaded from NASA's website (https://lpdaac.usgs.gov/products/mod17a3hv006/, accessed on 20 October 2020).

2.2.5. UGS Data

The UGS data of five cities in 2019 were obtained from the Aerospace Information Research Institute, Chinese Academy of Sciences. According to the classification standard of

UGS (CJJ/T85–2017) [38], this study focuses on four UGS types including the attached green space, park green space, protective green space, and regional green space. Furthermore, we divided the UGS into "UGS inside the urban built-up areas" and "UGS outside the urban built-up areas" to distinguish the differences. The data of urban built-up areas in five cities were retrieved from the dataset of built-up areas of Chinese cities developed by Sun et al. [39].

2.3. Methods

We optimized the traditional CASA model to calculate NPP values of UGS in five cities by specifying ε_{max} values of different vegetation types. The accuracy analysis was conducted to assess the performance of the NPP simulated model based on the MODIS NPP product. Then, the NEP was estimated by coupling the optimized CASA model and the semi-empirical model of soil heterotrophic respiration (R_H). Combining NEP and UGS data, we obtained the vegetation carbon sink capacity of different UGS types in 2019. The flowchart of the methodology is as follows (Figure 2).
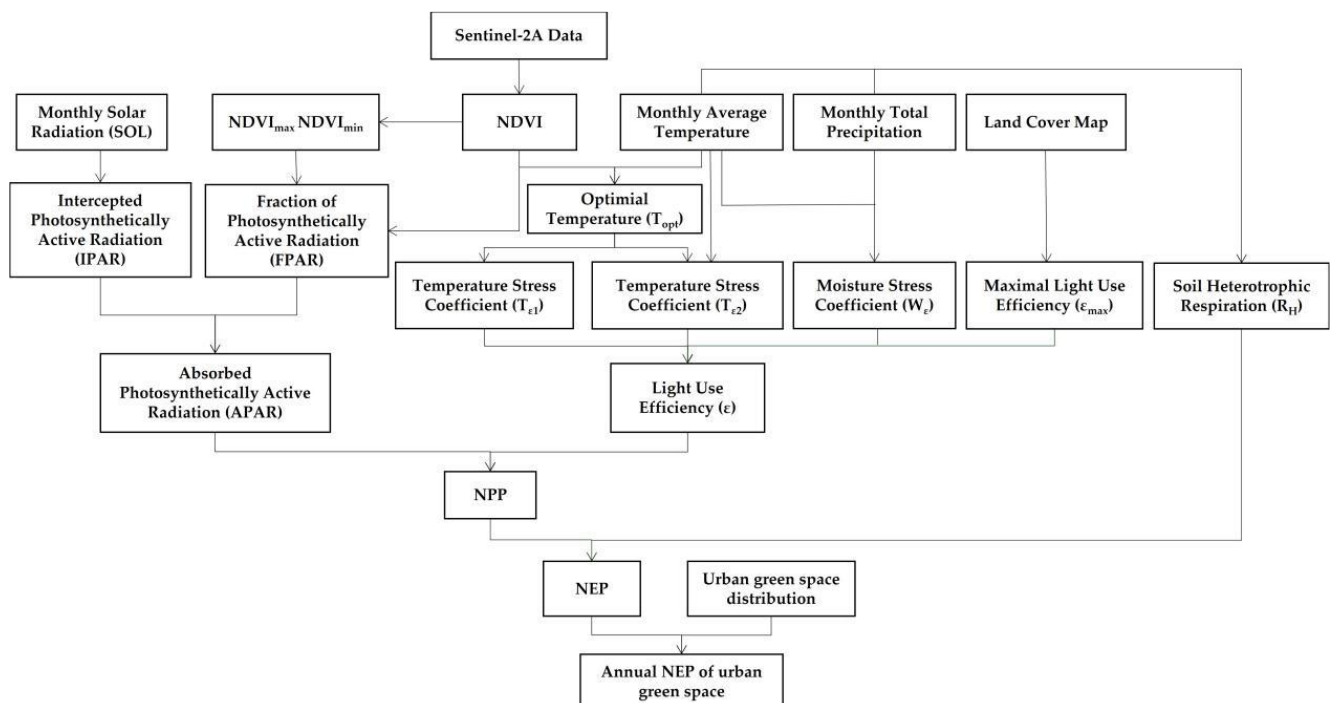
Figure 2. Flowchart of the methodology.

2.3.1. NPP Estimation Based on the Optimized CASA Model

The improved CASA model was adopted to simulate vegetation growth conditions, which considered vegetation growth characteristics and environmental conditions, and was able to more accurately determine the carbon source/sink attributes of the study area. The main algorithm of the model was integrated as follows [40]:

$$\text{NPP}(x,t) = 0.5 \times \text{SOL}(x,t) \times \text{FPAR}(x,t) \times T_{\varepsilon 1}(x,t) \times T_{\varepsilon 2}(x,t) \times W_{\varepsilon}(x,t) \times \varepsilon_{max} \qquad (2)$$

where the constant value 0.5 is the proportion of effective solar radiation (wavelength 0.4–0.7 μm) available to vegetation in total solar radiation, SOL(x,t) represents the total solar radiation, FPAR(x,t) is the proportion of photosynthetic active radiation absorbed by vegetation, $T_{\varepsilon 1}(x,t)$ and $T_{\varepsilon 2}(x,t)$ represent the stress effects of low and high temperature on light energy utilization, and $W_{\varepsilon}(x,t)$ is the water stress coefficient reflecting the influence of water conditions.

In a certain range, there is a linear relationship between FPAR and NDVI [41], which can be determined according to the maximum and minimum values of a certain type of NDVI and the corresponding maximum and minimum values of FPAR:

$$FPAR(x,t) = \frac{(NDVI(x,t) - NDVI_{i,min})}{(NDVI_{i,max} - NDVI_{i,min})} \times (FPAR_{max} - FPAR_{min}) + FPAR_{min} \quad (3)$$

where $NDVI_{i,max}$ and $NDVI_{i,min}$ correspond to the maximum and minimum NDVI values of the vegetation type, respectively. There is also a linear relationship between FPAR and the simple ratio (SR) [42], which can be expressed by the following formula:

$$FPAR(x,t) = \frac{(SR(x,t) - SR_{i,min})}{(SR_{i,max} - SR_{i,min})} \times (FPAR_{max} - FPAR_{min}) + FPAR_{min} \quad (4)$$

where the values of $FPAR_{min}$ and $FPAR_{max}$ are 0.001 and 0.95 irrespective of vegetation type. $SR_{i,max}$ and $SR_{i,min}$ correspond to 95% and 5% lower side percentiles of NDVI values, respectively, and $SR(x,t)$ is calculated by the following formula:

$$SR(x,t) = \frac{1 + NDVI(x,t)}{1 - NDVI(x,t)} \quad (5)$$

It is found that the FPAR estimated by NDVI is higher than the measured value, while the FPAR estimated by SR is lower than the measured value, but its error is smaller than that directly estimated by NDVI. Therefore, in this study, we combine the two methods and take the mean value as the estimated value of FPAR [43]:

$$FPAR(x,t) = (FPAR_{NDVI} + FPAR_{SR}) \times 0.5 \quad (6)$$

In order to improve the estimation accuracy of NPP values, we specified the previously unified ε_{max} values in the CASA model according to the vegetation types (Table 1) based on the MODIS MOD17 Biome Properties Look-Up Table (BPLUT) [25].

Table 1. Maximal LUE (ε_{max}) for different vegetation types.

Vegetation Type	ε_{max} (gC·MJ^{-1})
Deciduous needle leaf forest	1.086
Evergreen needle leaf forest	0.962
Deciduous broad leaf forest	1.165
Evergreen broad leaf forest	1.268
Mixed forest	1.051
Shrubland	1.061
Grassland	0.86
Cropland	1.044
Wetland	0.86

The estimation accuracy of the NPP estimation based on the optimized CASA model was tested by performing a linear regression between the estimated NPP values and the MOD17A3H Version 6 product.

2.3.2. NEP Estimation Method

NEP was calculated by the difference between NPP and R_H. Without considering the influence of other natural factors and human disturbance, NEP can represent the net carbon exchange between terrestrial ecosystems and atmospheric systems and is often used as a measure of carbon source/sink [44]. When the NEP value is greater than 0, it shows that the UGS functions as a carbon sink; otherwise, it is the carbon source. R_H can be calculated by the model established by [45]. The calculation method of NEP is as follows:

$$NEP = NPP - R_H \tag{7}$$

$$R_H = 0.22 \times \left[e^{(0.0913T)} + \ln(0.3145P + 1) \right] \times 30 \times 46.5\% \tag{8}$$

where T is the monthly average temperature and P is the monthly average precipitation.

2.3.3. Spatial Autocorrelation Analysis of NEP in UGS

Based on the Getis-Ord Gi* model and Moran's spatial autocorrelation model, the spatial distribution characteristics of NEP were analyzed.

Moran's spatial autocorrelation model was used to measure the degree of spatial autocorrelation at the same time according to the location and value of factors. Given a set of factors and related attributes, it should evaluate whether the mode is a cluster mode, discrete mode, or random mode. The clustering or discrete degree can be represented by calculating the value of Moran's I index. If the value of Moran's I index is regular, it indicates the clustering trend of factors. The higher the value, the greater the degree of positive correlation between factors. Furthermore, the Z-score and *p*-value were further calculated to evaluate the significance of the index [46]. If the value of Moran's I index is negative, it indicates that factors show a discrete trend: the smaller the value, the greater the degree of negative correlation between factors. If the value of Moran's I index is 0, it means that the spatial distribution of elements is random without clustering or discrete characteristics. Moran's I statistics of spatial autocorrelation can be expressed as:

$$I = \frac{\sum_{i=1}^{n} \sum_{j=1}^{n} w_{ij} z_i z_j}{\sum_{i=1}^{n} z_i^2} \times \frac{n}{S_0} \tag{9}$$

where z_i is the deviation between the attribute of element i and its mean value; w_{ij} is the spatial weight between element i and j; n is the total number of elements; and S_0 is the aggregation of spatial weights.

Expected index E(I) was used for comparison with Moran's I index:

$$E(I) = \frac{-1}{n - 1} \tag{10}$$

Variance Var(I) was used to evaluate the Z-score and *p*-value:

$$Var(I) = \frac{n^2 \frac{1}{2} \sum_{i=1}^{n} \sum_{j=1}^{n} \left(W_{ij} + W_{ij} \right)^2 - n \sum_{i=1}^{n} \left(\sum_{j=1}^{n} W_{ij} + \sum_{j=1}^{n} W_{ij} \right)^2 + 3S_0^2}{S_0^2(n^2 - 1)} \tag{11}$$

where W_{ij} is a member of the spatial weight matrix.

Score Z(I) represents the multiple of standard deviation. The higher the Z-score, the greater the degree of agglomeration or dispersion of elements. Z-scores are calculated in the following form:

$$Z(I) = \frac{1 - E(I)}{\sqrt{E\left(I^2\right) - E(I)^2}} \tag{12}$$

The *p*-value indicates the probability that the observed spatial pattern is created by some random process and is an approximation of the area derived from the curve of a known distribution (limited by test statistics). The smaller the *p*-value, the less randomness of the generated data, and the more valuable the research object.

The Getis-Ord G_i* model was used to spatially divide the hot and cold spots of NEP values. By calculating the Z-score and *p*-value of the significance level, which have obvious spatial statistical significance, the location of clustering of high or low value regions of NEP can be extracted in space using a 95% confidence interval [47].

$$G_i^* = \frac{\sum_{j=1}^{n} W_{ij} x_j}{\sum_{j=1}^{n} x_j} \tag{13}$$

$$Z\left(G_i^*\right) = \frac{\sum_{j=1}^{n} W_{ij}x_j - \overline{X}\sum_{j=1}^{n} W_{ij}}{\sqrt{\frac{s^2}{n-1}\left(n\sum_{j=1}^{n} W_{ij}^2 - \left(\sum_{j=1}^{n} W_{ij}\right)^2\right)}} \tag{14}$$

where x_j is NEP of pixel j, $\overline{X}$ is the mean of x_j, n is the total number of pixels, and s^2 is variance.

3. Results

3.1. NPP Analysis Based on the Optimized CASA Model

3.1.1. NPP Estimation Results

The spatial distribution of the NPP values of UGS in five cities in 2019 shows obvious differentiation (Figure 3). Among these cities, the average NPP value of UGS in Beijing is the highest (1008.5 gC·m^{-2}·a^{-1}) and the lowest average NPP value of UGS is in Shanghai (403.8 gC·m^{-2}·a^{-1}). The average NPP values of UGS in Guangzhou, Shenyang, and Xi'an are 997.4 gC·m^{-2}·a^{-1}, 666.1 gC·m^{-2}·a^{-1}, and 889.7 gC·m^{-2}·a^{-1}, respectively. The UGS with high NPP values is distributed in mountainous forest areas in the west and north of Beijing, Northeast Guangzhou, and South Xi'an, whereas the low NPP values of UGS are mostly distributed in the urban built-up area which is under strong anthropogenic influences.
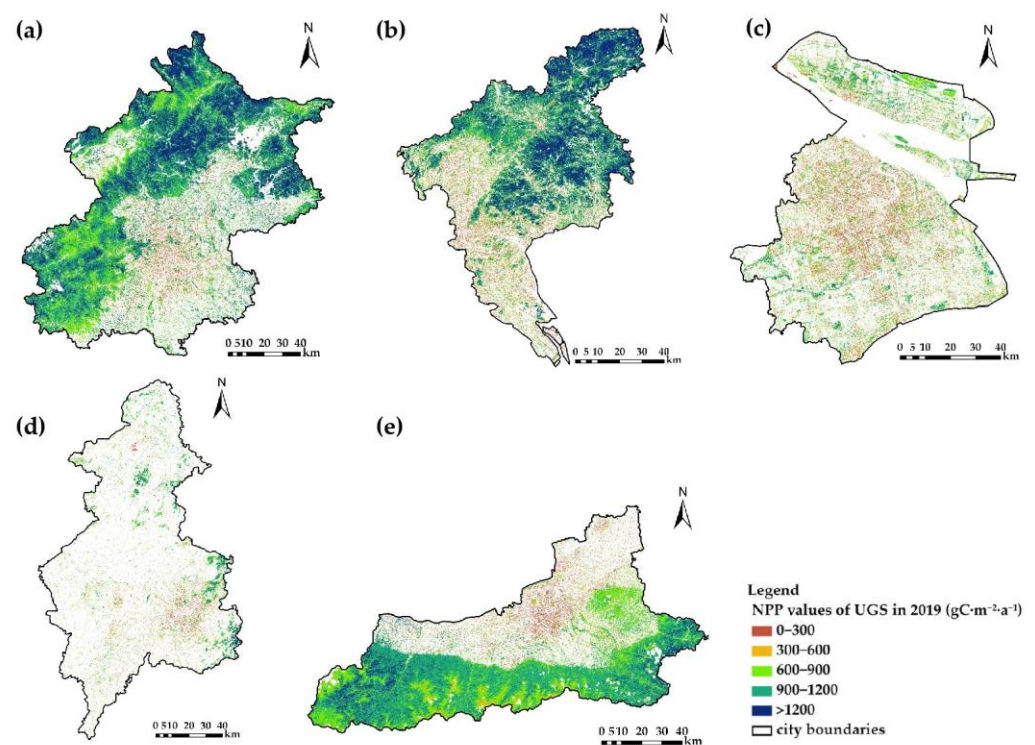
Figure 3. NPP value of UGS in five cities in 2019 ((**a**): Beijing, (**b**): Guangzhou, (**c**): Shanghai, (**d**): Shenyang, and (**e**): Xi'an).

The NPP values of UGS inside the urban built-up areas are much lower than the values outside the urban built-up areas (Table 2). Among the five cities, the UGS inside the urban built-up areas in Xi'an has the lowest NPP value (102.6 gC·m^{-2}·a^{-1}), whereas the value in Guangzhou is the highest (324.4 gC·m^{-2}·a^{-1}). For the UGS outside the urban built-up areas, the average NPP value is the highest in Guangzhou (1055.6 gC·m^{-2}·a^{-1}); however, Shanghai has the lowest value (650.7 gC·m^{-2}·a^{-1}).

Table 2. The average NPP values of UGS inside and outside the urban built-up areas in five cities in 2019 (gC·m^{-2}·a^{-1}).

UGS Location	Beijing	Guangzhou	Shanghai	Shenyang	Xi'an
UGS inside the urban built-up areas	227.0	324.4	212.7	204.2	102.6
UGS outside the urban built-up areas	1038.2	1055.6	650.7	725.8	912.4
total UGS	1008.5	997.4	403.8	666.1	889.7

3.1.2. NPP Values of Different UGS Types

Among all UGS types, the NPP values of regional green space are the highest, followed by park green space, while the NPP values of attached green space and protective green space are relatively low (Figure 4, Table 3). The NPP values of regional green space and park green space in Guangzhou rank first among the five cities, which are followed by the values in Beijing. As for the attached green space and the protective green space, the NPP values in Beijing are the highest and the values in Guangzhou came second. Although the average NPP value of total UGS in Xi'an is relatively high, the NPP values of attached green space, park green space, and protective green space in Xi'an are the lowest among the five cities.

Table 3. The average NPP values of different UGS types in five cities in 2019 (gC·m^{-2}·a^{-1}).

| UGS Type	Beijing	Guangzhou	Shanghai	Shenyang	Xi'an
attached green space	652.1	522.9	319.5	486.9	127.9
park green space	826.6	901.9	613.3	636.6	419.2
protective green space	609.0	425.6	384.5	301.1	122.7
regional green space	1067.7	1074.6	705.9	728.3	918.5
total UGS	1008.5	997.4	403.8	666.1	889.7

Among the UGS inside the urban built-up areas, the park green space is the UGS type with the highest NPP value, whereas the attached green space has the lowest NPP values in five cities (Table 4). All the UGS types outside the urban built-up areas have higher NPP values than the same UGS types inside the urban built-up areas (Table 5). The regional green space is the UGS type with the highest NPP value outside the urban built-up areas, which is followed by park green space. The NPP values of attached green space and protective green space are relatively lower than the other UGS types outside the urban built-up areas.

Table 4. The average NPP values of different UGS types inside the urban built-up areas in five cities in 2019 (gC·m^{-2}·a^{-1}).

UGS Type	Beijing	Guangzhou	Shanghai	Shenyang	Xi'an
attached green space	200.5	313.7	194.8	151.4	80.3
park green space	452.1	484.5	500.1	595.5	393.1
protective green space	300.2	323.8	294.0	205.6	94.5
regional green space	295.1	335.5	269.1	247.1	170.7

Table 5. The average NPP values of different UGS types outside the urban built-up areas in five cities in 2019 (gC·m^{-2}·a^{-1}).

UGS Type	Beijing	Guangzhou	Shanghai	Shenyang	Xi'an
attached green space	809.8	761.2	485.7	674.0	245.7
park green space	867.8	973.0	686.0	691.3	488.2
protective green space	721.1	612.2	517.5	456.3	202.8
regional green space	1068.5	1079.2	719.0	739.4	919.7
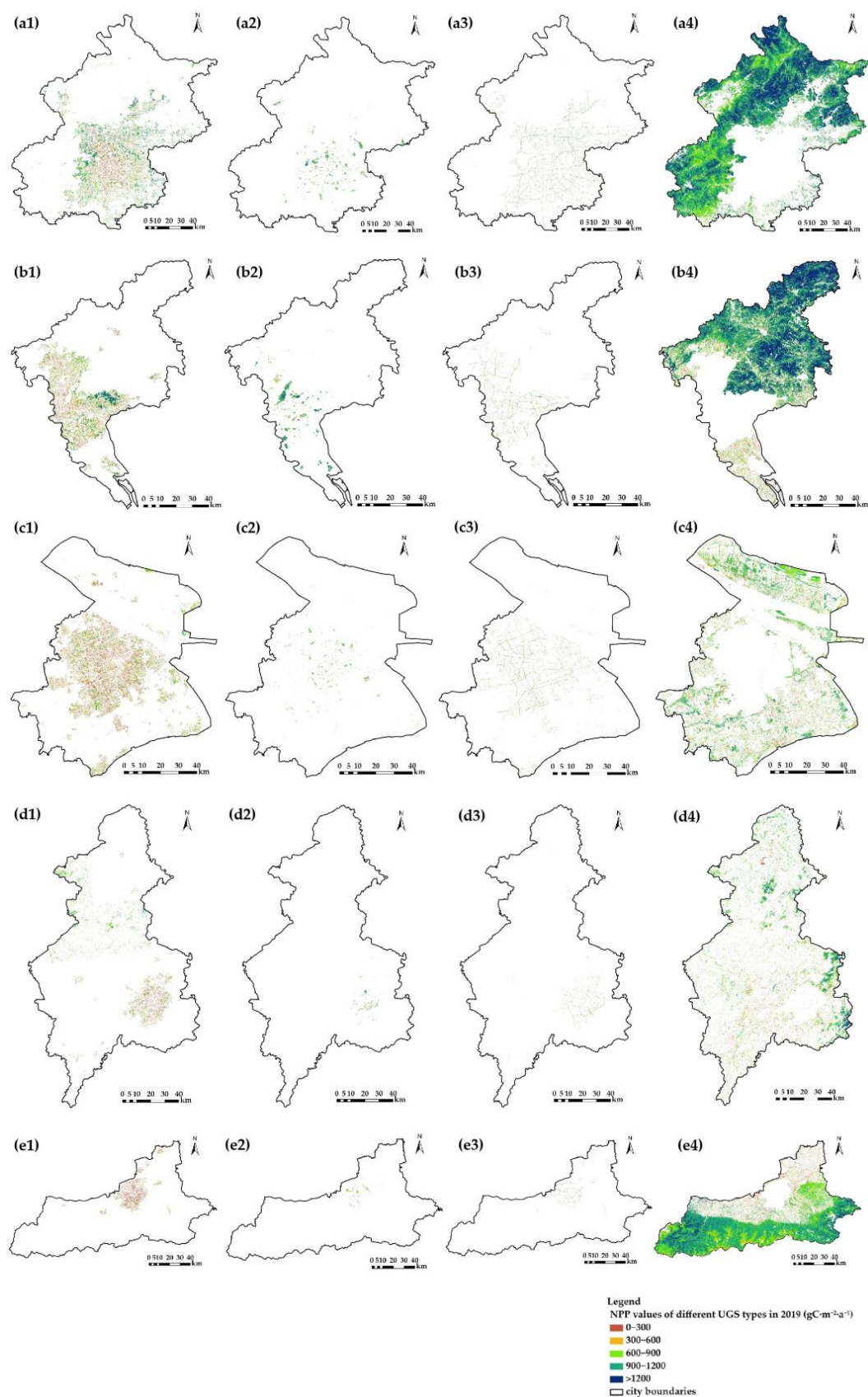
Figure 4. The spatial distribution of NPP values of different UGS in five cities in 2019 ((**a**): Beijing, (**b**): Guangzhou, (**c**): Shanghai, (**d**): Shenyang, and (**e**): Xi'an and 1: attached green space, 2: park green space, 3: protected green space, and 4: regional green space).

3.1.3. The Accuracy Test of Estimated NPP Values

MOD17A3H data were used to verify the NPP estimation accuracy. This product has a wide range of applications in NPP research at different spatial scales and it is available only as an annual product [48]. The estimated NPP values of each UGS type were compared with the MOD17A3H data with the linear regression model. Most of the coefficients of determination, R^2, are greater than 0.5 (Table 6), which indicates that the accuracy of the estimated values of UGS based on the optimized CASA model is high and the linear relationship between the estimated NPP and the MODIS NPP values is distinct.

**Table 6.** Coefficient of determination, R^2, of the linear regression model.

UGS Type	Beijing	Guangzhou	Shanghai	Shenyang	Xi'an
attached green space	0.658 **	0.708 **	0.496 **	0.819 **	0.509 **
park green space	0.631 **	0.677 **	0.339 **	0.275 **	0.617 **
protective green space	0.534 **	0.572 **	0.503 **	0.603 **	0.542 **
regional green space	0.900 **	0.924 **	0.807 **	0.918 **	0.955 **
total UGS	0.875 **	0.903 **	0.730 **	0.897 **	0.951 **

**: p-value < 0.01.

3.2. The NEP Values of UGS in Different Cities

3.2.1. The Spatial Distribution of NEP of UGS

Figure 5 shows the spatial distribution of NEP values in UGS in 2019.
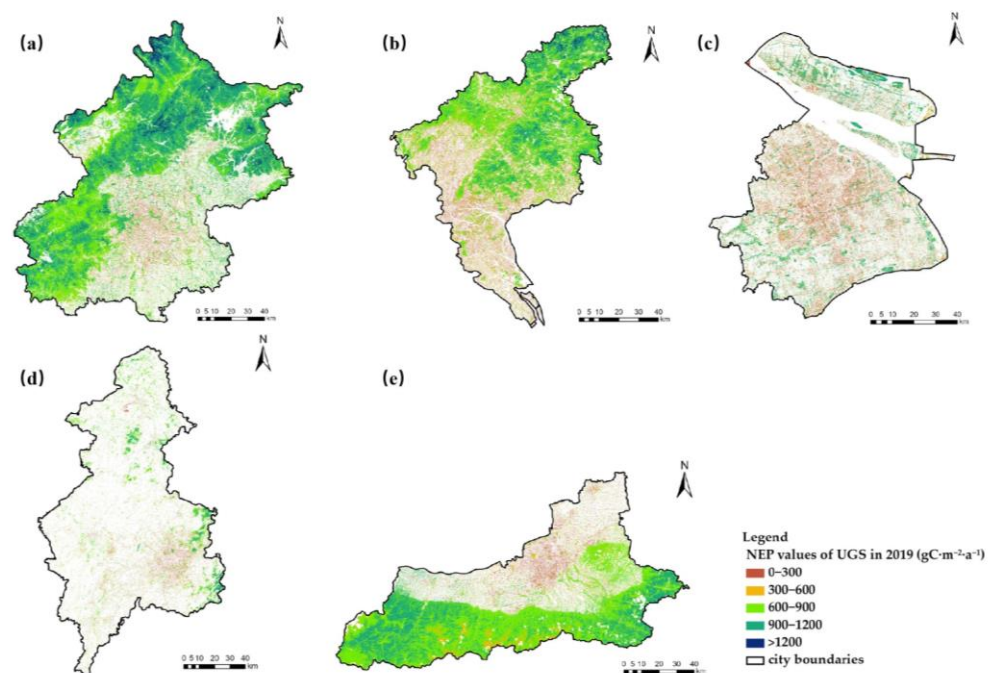
Figure 5. NEP values of UGS in five cities in 2019 ((**a**): Beijing, (**b**): Guangzhou, (**c**): Shanghai, (**d**): Shenyang, and (**e**): Xi'an).

According to the spatial distribution of NEP values (Table 7), UGS of Beijing has the highest annual average NEP value (771.5 gC·m^{-2}·a^{-1}) and is followed by Xi'an (632.7 gC·m^{-2}·a^{-1}), whereas UGS of Shanghai has the lowest NEP value (194.2 gC·m^{-2}·a^{-1}). The average NEP values of UGS inside the urban built-up areas in five cities are all negative, whereas UGS outside the urban built-up areas are positive. Among the five cities, the UGS inside the urban built-up areas in Xi'an has the lowest NEP value (−162.1 gC·m^{-2}·a^{-1}), whereas, the value in Shenyang is the highest (−19.4 gC·m^{-2}·a^{-1}). For the UGS outside the urban built-up areas, the average NEP value is the highest in Beijing (802.0 gC·m^{-2}·a^{-1}); however, Shanghai has the lowest NEP value (306.7 gC·m^{-2}·a^{-1}).

Table 7. The average NEP values of UGS inside and outside the urban built-up areas in five cities in 2019 (gC·m^{-2}·a^{-1}).

UGS Location	Beijing	Guangzhou	Shanghai	Shenyang	Xi'an
UGS inside the urban built-up areas	−28.8	−115.7	−135.4	−19.4	−162.1
UGS outside the urban built-up areas	802.0	625.7	306.7	505.0	655.6
total UGS	771.5	566.7	194.2	445.0	632.7

Among all UGS types, regional green space has the highest NEP values, which is followed by park green space, whereas, the NEP values of attached green space and protective green space are relatively low (Table 8). Most NEP values of UGS are positive, indicating that they are overall carbon sinks. However, the NEP values of the attached green space in Shanghai and Xi'an are −27.74 gC·m^{-2}·a^{-1} and −137.62 gC·m^{-2}·a^{-1}. Furthermore, the NEP values of protective green space in Guangzhou and Xi'an are negative at −14.49 gC·m^{-2}·a^{-1} and −140.53 gC·m^{-2}·a^{-1}, which means that vegetation carbon storage is lower than soil microbial respiration in these areas and the ecosystem of protective green space functions as a carbon source.

Table 8. The average NEP values of different UGS types in five cities in 2019 (gC·m^{-2}·a^{-1}).

UGS Type	Beijing	Guangzhou	Shanghai	Shenyang	Xi'an
attached green space	399.1	82.7	−27.7	265.8	−137.6
park green space	572.2	460.2	266.8	413.1	189.6
protective green space	355.7	−14.5	36.2	77.6	−140.5
regional green space	833.4	645.6	362.6	507.6	661.7
total UGS	771.5	566.7	194.2	445.0	632.7

Among the UGS inside the urban built-up areas, the attached green space has the lowest and most negative NEP values (Table 9). The park green space inside the urban built-up areas has the highest and most positive NEP values. The protective green space inside the urban built-up areas in Beijing and the regional green space inside the urban built-up areas in Beijing and Shenyang have positive NEP values.

Table 9. The average NEP values of different UGS types inside the urban built-up areas in five cities in 2019 (gC·m^{-2}·a^{-1}).

| UGS Type	Beijing	Guangzhou	Shanghai	Shenyang	Xi'an
attached green space	−55.4	−126.3	−153.3	−72.3	−184.3
park green space	195.5	44.4	152.6	371.9	134.9
protective green space	44.4	−116.2	−54.3	−18.1	−169.9
regional green space	42.9	−106.3	−79.2	23.6	−95.0

Most of the UGS outside the urban built-up areas have positive NEP values except the attached green space (−14.6 gC·m^{-2}·a^{-1}) and protective green space (−56.6 gC·m^{-2}·a^{-1}) in Xi'an (Table 10). Among the UGS outside the urban built-up areas in all cities, the regional green space has the highest NEP values, which is followed by the park green space.

Comparing the NEP distribution in UGS in different cities (Figure 6), it can be seen that the carbon source area in UGS in Shanghai covers 32.51% of the UGS area, whereas, the carbon source area accounts for 4.53% and 5.89% of the UGS in Beijing and Xi'an. In Beijing, 47.36% of UGS has a relatively high NEP value (800 to 1200 gC·m^{-2}·a^{-1}); however, NEP values of UGS in other cities are mainly concentrated in the medium range (400 to 800 gC·m^{-2}·a^{-1}). About 4.16% of UGS in Beijing has a NEP value of higher than 1200 gC·m^{-2}·a^{-1}.

Table 10. The average NEP values of different UGS types outside the urban built-up areas in five cities in 2019 (gC·m^{-2}·a^{-1}).

UGS Type	Beijing	Guangzhou	Shanghai	Shenyang	Xi'an
attached green space	557.8	320.8	139.4	454.3	−14.6
park green space	613.6	531.0	340.1	467.9	235.3
protective green space	468.6	171.7	169.4	233.1	−56.6
regional green space	834.3	650.4	375.9	518.7	662.9
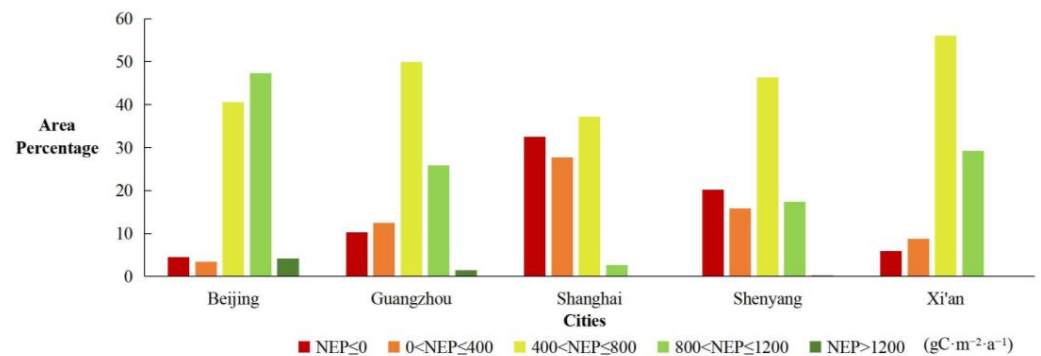
Figure 6. The proportion of UGS at each level of annual average NEP value in five cities in 2019.

3.2.2. Spatial Autocorrelation Analysis of NEP Values

Global autocorrelation analysis of NEP values of total UGS in different cities was conducted to explore the aggregation and dispersion characteristics of vegetation carbon sink capacity. Table 11 shows that the detection results of the degree of randomness of the data are all less than 0.01 and the corresponding *p*-values are all 0, indicating that the probability of each element data being generated randomly is very small and it has passed the randomness test. The Z scores of NEP in all the cities are much higher than the discriminant value of aggregation characteristics ($Z(I) > 2.58$). Therefore, the spatial distribution of vegetation carbon sink capacity of UGS presents the characteristics of high aggregation. Moran's I index is between 0.22 and 0.56, indicating that the NEP of UGS has an obvious positive spatial correlation, that is, vegetation carbon sink capacity presents the characteristics of "high aggregation" or "low aggregation" on the whole.

Table 11. Global autocorrelation results of NEP of total UGS in different cities.

Cities	Moran's I	E(I)	Var(I)	Z(I)	*p*
Beijing	0.42	−0.000097	0.000011	129.50	0
Guangzhou	0.44	−0.000225	0.000022	93.96	0
Shanghai	0.22	−0.000523	0.000049	31.28	0
Shenyang	0.31	−0.000858	0.000071	37.42	0
Xi'an	0.56	−0.000167	0.000011	168.24	0

From the above global spatial autocorrelation analysis, it can be seen that in terms of spatial distribution characteristics, the vegetation carbon sink capacity of UGS in all cities has a high degree of spatial autocorrelation and the overall pattern is spatial agglomeration. The Getis-Ord G$_i$* model was conducted in order to further explore the location of such agglomeration characteristics as well as the hot and cold spot spatial distribution areas of NEP in different cities.

Figure 7 shows the hot spot analysis results of the vegetation carbon sink capacity of UGS in five cities. It can be seen from the results that the spatial distribution of hot and cold spots of vegetation carbon sink capacity varies in different cities. With a confidence interval greater than 95% as the evaluation criteria, the hot spots of vegetation carbon sink capacity are mainly distributed in the north and west of Beijing, in the north and east of

Guangzhou and Shenyang, in the north and south of Shanghai, and in the west and east of Xi'an. The cold spots are mainly distributed in the central and southern part of Beijing, in the west and south of Guangzhou, in the central part of Shanghai, in the south of Shenyang, and in the north and south part of Xi'an.
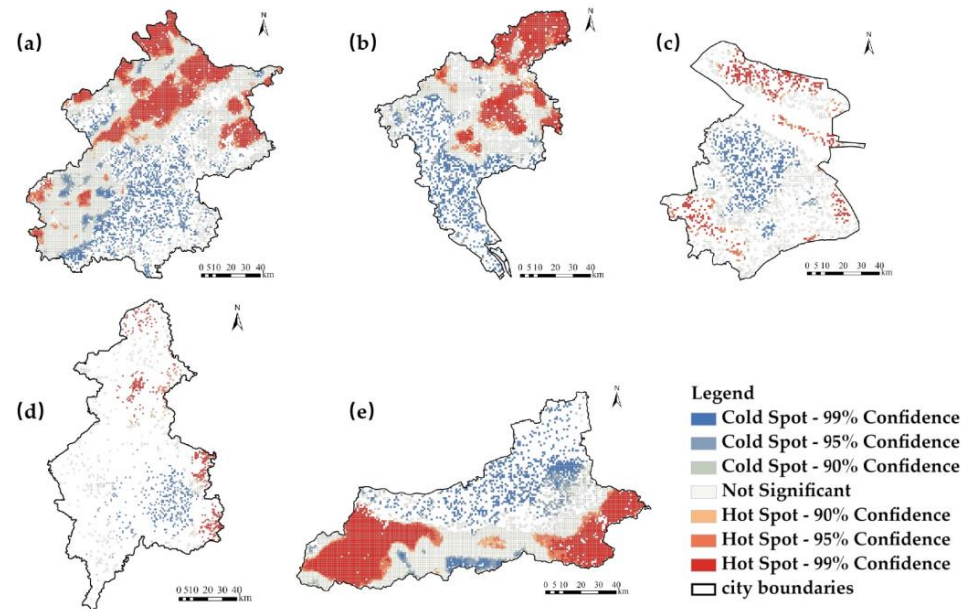
Figure 7. Cold-and hot-spots spatial variations of NEP values of UGS in five cities ((**a**): Beijing, (**b**): Guangzhou, (**c**): Shanghai, (**d**): Shenyang, and (**e**): Xi'an).

The cluster and outlier distribution of NEP (Figure 8) is similar to that of hot and cold spots. These results indicate that the spatial distribution of NEP of UGS in five cities mainly presents high–high aggregation and low–low aggregation, that is, areas with high/low NEP values are more clustered in space. High–high aggregation is mainly distributed in hot spot areas (Figure 7), while low–low aggregation is mainly distributed in eastern cold spot areas (Figure 7). However, there are few high–low aggregation and low–high aggregation areas.
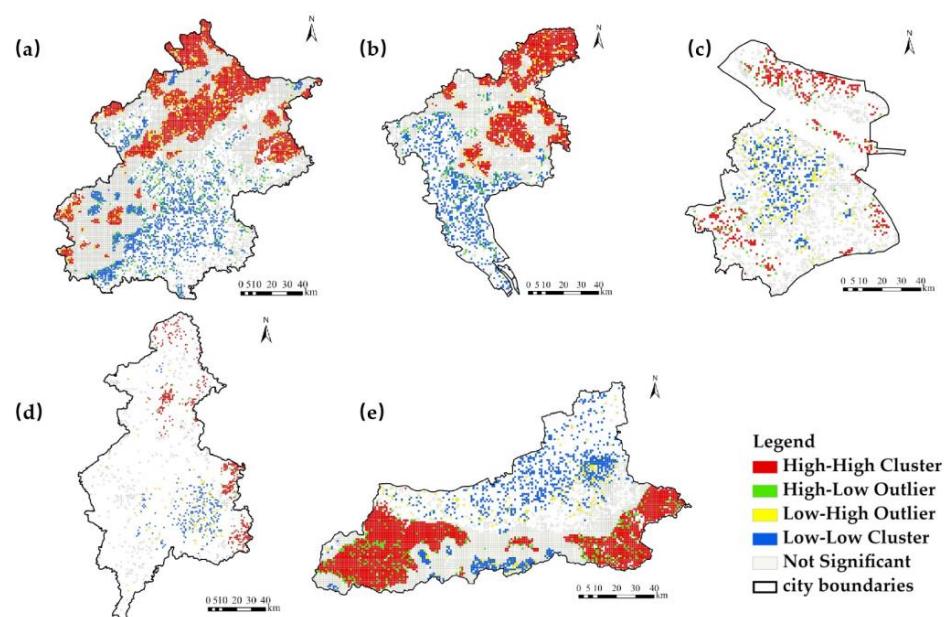
Figure 8. Cluster and outlier of NEP values of UGS in five cities ((**a**): Beijing, (**b**): Guangzhou, (**c**): Shanghai, (**d**): Shenyang, and (**e**): Xi'an).

4. Discussion

4.1. The NPP Estimation of UGS

Since it is difficult to obtain the measured NPP data of UGS in these cities, the estimated NPP values of the optimized CASA model were fitted with MOD17A3HGF products to verify the model accuracy. The results show that the estimated results have a strong correlation with MODIS NPP values, indicating that the optimized model can be used to calculate the NPP of UGS effectively and provide basic data for further study. However, the estimated values are higher than that of MOD17A3HGF products, which is because the MOD17A3HGF products underestimate the productivity of shrubs and grassland but fit well with other vegetation types [49].

The spatial distribution of NPP values of UGS varies in different cities. Among the five cities, UGS in Beijing has the highest NPP and NEP values than in the other cities, which is closely related to the measures Beijing has taken in recent years to reduce carbon emissions and increase carbon sequestration. Based on the functional positioning of different regions, the government has taken into account factors such as the level of economic and social development, resource endowment, and emission reduction potential to explore the paths of realizing carbon peaking and carbon neutrality. The high NPP area in Beijing is mostly distributed in the ecological conservation areas, which are the important ecological barrier and water source protection areas of Beijing [50]. This result is similar to Peng's research [19] which found that the NPP values were higher in the northern and northwestern mountains than on the plains in Beijing. In recent years, green space has been continuously expanded and forest coverage has continued to increase through the implementation of a new round of million acres of afforestation project and the second phase of the Beijing–Tianjin sandstorms control project. In Guangzhou, most of the high-NPP UGS area are distributed in the mountainous forests in Conghua, Huadu, and Zengcheng Mountains in the north of Guangzhou, which is the area with the most concentrated number of natural protected areas, the most abundant natural resources, and the highest biodiversity in Guangzhou [51]. With water conservation and biodiversity protection as the main ecological functions, it is the urban ecological protection screen in the north of Guangzhou. This finding is in agreement with Wu's study [52] which demonstrated the spatial heterogeneity of NPP between urban and forested areas in Guangzhou. The high NPP values in Shanghai are mainly distributed in the Chongming District which is rich in ecological resources. It is an important protection area for the diversity of natural resources in the world and an important habitat for birds. It is also a demonstration area for the ecological environment protection of the Yangtze River and a pilot area for the development of national ecological civilization [53]. Eisfelder [54] found the low NPP values around the city center of Shanghai, which can be explained by the high urban sprawl in that area. In Shenyang, the high NPP values are mainly distributed in the ecological source of the hilly area in the southeast and northeast, which carries important functions such as water conservation and biodiversity protection. In the previous study of the Shenyang metropolitan area [55], the conversion of farmland to urban land and the loss of forest land from 2000–2010 caused the reduction in average NPP values. The high NPP values are distributed in the south of Xi'an, which is the ecological barrier at the northern foot of the Qinling Mountains. With a forest coverage rate of 71%, it is the most bio-diverse area in the Yellow River Basin with more than 1800 seed plants and 470 vertebrates including 17 state key protection plants and 79 state class I and II protection wild animals. This area plays an important role in climate regulation, water source regulation, carbon sequestration, and oxygen release. The results are in accordance with the study on NPP in Guanzhong Plain from 2000 to 2019, which shows the high NPP values in the Qinling Mountains and low values in the urban area; it found that the spatial distribution of NPP values is consistent with the distribution pattern of precipitation [56].

Among all types of green space, in the whole urban area, the NPP values of regional green space are the highest, followed by park green space, while the NPP values of attached green space and protective green space are relatively low. This result can be verified by existing studies, which have clarified the difference in carbon sink capacity of different

green space types. The carbon sink capacity of vegetation, soil, and litter is different under different land use modes. Generally speaking, regional green space is higher than other types of green space. Zhu et al. demonstrated that the carbon sink capacity of park green space dominated by leisure and sports is higher than that of protective green space and attached green space [57]. Moreover, human influence also has a huge impact on the carbon sink capacity of UGS, therefore, the carbon sink capacity of ecological-conservation-oriented UGS is obviously greater than that of other UGS types. For the UGS inside the urban built-up areas, the park green space has the highest NPP values, while the NPP values of the attached green space is the lowest. The UGS outside the urban built-up areas show higher NPP values than UGS inside the built-up areas. Regional green space is usually located outside urban built-up areas, which has the functions of protecting the urban and rural ecological environment, natural resources and cultural resources, recreation and fitness, safety protection and isolation, species protection, and garden seedling production. It plays an important role in maintaining urban and rural ecological security and promoting the sustainable development of human society.

4.2. The NEP Estimation Results of the Coupling Model

Without considering other natural factors and human disturbance, vegetation NEP can represent the net carbon exchange between terrestrial ecosystems and atmospheric systems [58]. In this study, NEP values were estimated by coupling the optimized CASA model and the semi-empirical soil respiration model. The results show that most NEP values of UGS are positive, indicating that they are overall carbon sinks. However, the NEP values of the attached green space in Shanghai and Xi'an, as well as the protective green space in Guangzhou and Xi'an are negative, indicating that these areas are basically carbon sources. Comparing the NEP results of UGS inside and outside the urban built-up areas, we find that the NEP values of the UGS type inside the urban built-up areas are all lower than the same UGS type outside the built-up areas. Only the park green space inside the urban built-up areas have positive NEP values in five cities; the other UGS types including the attached green space, protective green space, and regional green space mainly have negative NEP values inside the urban built-up areas. Therefore, it is essential to improve the carbon sink capacity of UGS, especially the attached green space and the protective green space, inside the urban built-up areas. According to Huang's study in Guangzhou, the green space in parks and densely planted forest areas are carbon sinks, while the roadside green spaces mostly present carbon source characteristics; the carbon source-sink characteristics of urban green spaces will change with the increase in green space age [59]. Yang et al. also demonstrated that the UGS type has an indirect effect on the carbon pool of regional urban green space [60]. Due to the differences in green coverage rate, hard surface ratio, other indicators of different UGS types, and the regional characteristics in different cities, the proportion of surface soil organic carbon density and vegetation carbon density in different UGS types present strong heterogeneity [61,62]. The carbon pool of different types of urban green space under the influence of multiple factors shows the characteristics of a carbon source or carbon sink.

The vegetation carbon sink capacity of UGS in five cities shows a high degree of spatial autocorrelation and the overall pattern was spatial agglomeration. On the whole, the low–low clusters especially the area with negative NEP values are mainly close to urban industrial and mining land with low vegetation coverage, where human activities have a negative impact on the ecosystem productivity. The high–high clusters gather in areas with rich soil and complex vegetation types with suitable temperatures and precipitation for plant growth.

4.3. The Prospects of the Study

Model validation is the key to estimating biomass in large-scale regions. In this study, the revised CASA model and soil microbial respiration model were used to estimate the vegetation carbon sink capacity of UGS in Chinese cities but the following uncertainties

still exist. Firstly, the accuracy of NPP was verified by comparison with MODIS NPP data and other research results but no measured data were obtained. Secondly, NEP is indirectly verified based on the results of NPP and R_H but the accuracy of NEP is not directly verified. Thirdly, despite the modification of CASA model parameters, long-time scale observation has not been carried out which needs to be conducted in a further study.

5. Conclusions

Based on high-resolution satellite images and meteorological data, we improved the traditional CASA model and explored the spatial distribution of vegetation NPP and NEP of different UGS types in five typical cities in China in 2019. The following conclusions were obtained:

(1) The optimized CASA model with high-resolution satellite images and a specified ε_{max} for different vegetation types is an effective method to estimate the NPP values of UGS. Among the selected cities, Beijing has the best performance in terms of NPP and vegetation carbon sink capacity due to the sound ecological protection and low-carbon management measures;

(2) The vegetation NPP and vegetation carbon sink capacity of different UGS types in five cities have similar characteristics, that is, in the urban area NPP and NEP values of regional green space are the highest, which are followed by the values of park green space, while the NPP and NEP values of attached green space and protective green space are relatively low. The UGS inside the urban built-up areas have lower NPP and NEP values than the UGS outside the urban built-up areas. It is especially essential to improve the carbon sink capacity of attached green space and protective green space inside the urban built-up areas;

(3) The NEP values estimated by the coupling model of the optimized CASA model and the soil heterotrophic respiration model indicate that most of the UGS types are carbon sinks. However, the attached green space in Shanghai and Xi'an and the protective green space in Guangzhou and Xi'an are carbon sources. Effective measures to reduce carbon emissions and increase carbon sequestration should be taken for these carbon source areas;

(4) The NEP values of UGS are different in each region of China, presenting the pattern of Beijing > Xi'an > Guangzhou > Shenyang > Shanghai. In all five cities, the spatial distribution of NEP values shows a high degree of spatial autocorrelation. The areas with high–high clusters should be protected and the connectivity of the UGS network should be increased in order to improve the vegetation carbon sink capacity of the UGS ecosystem.

References

1. Zhang, W.; Huang, B.; Luo, D. Effects of Land Use and Transportation on Carbon Sources and Carbon Sinks: A Case Study in Shenzhen, China. *Landsc. Urban Plann.* **2014**, *122*, 175–185. [CrossRef]
2. Chuai, X.; Huang, X.; Lu, Q.; Zhang, M.; Zhao, R.; Lu, J. Spatiotemporal Changes of Built-Up Land Expansion and Carbon Emissions Caused by the Chinese Construction Industry. *Env. Sci. Technol.* **2015**, *49*, 13021–13030. [CrossRef] [PubMed]
3. Strohbach, M.W.; Arnold, E.; Haase, D. The Carbon Footprint of Urban Green Space—A Life Cycle Approach. *Landscape Urban Plann.* **2012**, *104*, 220–229. [CrossRef]
4. Nowak, D.J.; Greenfield, E.J.; Hoehn, R.E.; Lapoint, E. Carbon Storage and Sequestration by Trees in Urban and Community Areas of the United States. *Environ. Pollut.* **2013**, *178*, 229–236. [CrossRef] [PubMed]
5. Grimmond, C.S.B.; King, T.S.; Cropley, F.D.; Nowak, D.J.; Souch, C. Local-Scale Fluxes of Carbon Dioxide in Urban Environments: Methodological Challenges and Results from Chicago. *Environ. Pollut.* **2002**, *116*, 243–254. [CrossRef]
6. Chang, S.; Yang, H.; Ge, J. Research Progress and Problems of Net Ecosystem Productivity. *J. Beijing Norm. Univ. (Nat. Sci. Ed.)* **2005**, *5*, 517–521.
7. Mu, S.; Zhou, K.; Chen, Y.; Yang, Q.; Li, J. Dynamic Changes of Net Ecosystem Productivity of Different Communities in Typical Grasslands of Inner Mongolia. *J. Ecol.* **2014**, *33*, 885–895.
8. Field, C.B. Sharing the Garden. *Science* **2001**, *294*, 2490–2491. [CrossRef]
9. Xing, W.; Chi, Y.; Ma, X.; Liu, D. Spatiotemporal Characteristics of Vegetation Net Primary Productivity on an Intensively-Used Estuarine Alluvial Island. *Land* **2021**, *10*, 130. [CrossRef]
10. Lieth, H. Modeling the Primary Productivity of the World. In *Primary Productivity of the Biosphere*; Lieth, H., Whittaker, R.H., Eds.; Springer: Berlin, Germany, 1975; pp. 237–263.
11. Lieth, H. Evapotranspiration and Primary Productivity; C.W. THORNTHWAITE Memorial Mode. *Publ. Climatol.* **1972**, *25*, 37–46.
12. Uchijima, Z.; Seino, H. Agroclimatic Evaluation of Net Primary Productivity of Natural Vegetations. *J. Agric. Meteorol.* **1985**, *40*, 343–352. [CrossRef]
13. White, M.A.; Thornton, P.E.; Running, S.W.; Nemani, R.R. Parameterization and Sensitivity Analysis of the BIOME–BGC Terrestrial Ecosystem Model: Net Primary Production Controls. *Earth Interact.* **2000**, *4*, 1–85. [CrossRef]
14. Potter, C.S.; Randerson, J.T.; Field, C.B.; Matson, P.A.; Vitousek, P.M.; Mooney, H.A.; Klooster, S.A. Terrestrial ECOSYSTEM Production: A Process Model Based on Global Satellite and Surface Data. *Global Biogeochem. Cycles* **1993**, *7*, 811–841. [CrossRef]
15. Zhou, K.-S.; Du, J.; Shen, X.; Pu, G.-J.; Zhang, D.-D.; Dang, X.-N. Spatial and Temporal Variability of Vegetation Net Primary Productivity in Qiangtang National Nature Reserve under Climate Change. *Chin. J. Agrometeorol.* **2021**, *42*, 627–641.
16. Chuanhua, L.; Haiyan, H.; Yeping, F.; Hongjuan, C.; Yutao, W.; Hao, S. NPP Change and Scenario Simulation in Wudaoliang Area of the Tibetan Plateau Based on Biome-BGC Model. *Sci. Geogr. Sin.* **2019**, *39*, 1330–1339.
17. Zhang, Y.; Hao, H.; Fan, L.; Li, Y.; Zhang, R.; Li, K. Study on Spatio-Temporal Dynamics and Driving Factors of NPP in Central Asian Grassland. *Arid. Zone Res.* **2022**, *39*, 698–707.
18. Zhou, W.; Mu, F.; Gang, C.; Guan, D.; He, J.; Li, J. Spatio-Temporal Dynamics of Grassland Net Primary Productivity and their Relationship with Climatic Factors from 1982 to 2010 in China. *Acta Ecol. Sin.* **2017**, *37*, 4335–4345.
19. Peng, J.; Shen, H.; Wu, W.; Liu, Y.; Wang, Y. Net Primary Productivity (NPP) Dynamics and Associated Urbanization Driving Forces in Metropolitan Areas: A Case Study in Beijing City, China. *Landscape Ecol.* **2016**, *31*, 1077–1092. [CrossRef]
20. Gao, Q.; Wan, Y.; Li, Y.; Guo, Y.; Ganjurjav; Qin, X.; Jiangcun, W.; Wang, B. Effects of Topography and Human Activity on the Net Primary Productivity (NPP) of Alpine Grassland in Northern Tibet from 1981 to 2004. *Int. J. Remote Sens.* **2013**, *34*, 2057–2069. [CrossRef]
21. Yu, R. An Improved Estimation of Net Primary Productivity of Grassland in the Qinghai-Tibet Region Using Light Use Efficiency with Vegetation Photosynthesis Model. *Ecol. Model.* **2020**, *431*, 109–121. [CrossRef]
22. Dong, G.; Bai, J.; Yang, S.; Wu, L.; Cai, M.; Zhang, Y.; Luo, Y.; Wang, Z. The Impact of Land Use and Land Cover Change on Net Primary Productivity on China's Sanjiang Plain. *Environ. Earth Sci.* **2015**, *74*, 2907–2917. [CrossRef]
23. Liang, L.; Geng, D.; Yan, J.; Qiu, S.; Shi, Y.; Wang, S.; Wang, L.; Zhang, L.; Kang, J. Remote Sensing Estimation and Spatiotemporal Pattern Analysis of Terrestrial Net Ecosystem Productivity in China. *Remote Sens.* **2022**, *14*, 1902. [CrossRef]
24. Fisher, J.B.; Sikka, M.; Oechel, W.C.; Huntzinger, D.N.; Melton, J.R.; Koven, C.D.; Ahlström, A.; Arain, M.A.; Baker, I.; Chen, J.M.; et al. Carbon Cycle Uncertainty in the Alaskan Arctic. *Biogeosciences* **2014**, *11*, 4271–4288. [CrossRef]
25. Running, S.W.; Zhao, M. Daily GPP and Annual NPP (MOD17A2/A3) Products NASA Earth Observing System MODIS Land Algorithm. *MOD17 User's Guide* **2015**, *2015*, 1–28.
26. Bala, G.; Joshi, J.; Chaturvedi, R.K.; Gangamani, H.V.; Hashimoto, H.; Nemani, R. Trends and Variability of AVHRR-Derived NPP in India. *Remote Sens.* **2013**, *5*, 810–829. [CrossRef]
27. Yan, Y.; Liu, X.; Wang, F.; Li, X.; Ou, J.; Wen, Y.; Liang, X. Assessing the Impacts of Urban Sprawl on Net Primary Productivity Using Fusion of Landsat and MODIS Data. *Sci. Total Environ.* **2018**, *613*, 1417–1429. [CrossRef]
28. Robinson, N.P.; Allred, B.W.; Smith, W.K.; Jones, M.O.; Moreno, A.; Erickson, T.A.; Naugle, D.E.; Running, S.W. Terrestrial Primary Production for the Conterminous United States Derived from Landsat 30 m and MODIS 250 m. *Remote Sens. Ecol. Conserv.* **2018**, *4*, 264–280. [CrossRef]
29. He, L.; Wang, R.; Mostovoy, G.; Liu, J.; Chen, J.M.; Shang, J.; Liu, J.; McNairn, H.; Powers, J. Crop Biomass Mapping Based on Ecosystem Modeling at Regional Scale Using High Resolution Sentinel-2 Data. *Remote Sens.* **2021**, *13*, 806. [CrossRef]

30. Aklilu, D.; Wang, T.; Amsalu, E.; Feng, W.; Li, Z.; Li, X.; Tao, L.; Luo, Y.; Guo, M.; Liu, X.; et al. Short-Term Effects of Extreme Temperatures on Cause Specific Cardiovascular Admissions in Beijing, China. *Environ. Res.* **2020**, *186*, 109455. [CrossRef]
31. Overview of Beijing. Available online: https://www.beijing.gov.cn/renwen/bjgk/#dlyzr (accessed on 11 January 2023).
32. General Situation of Guangzhou. Available online: https://www.gz.gov.cn/zlgz/gzgk/zrdl/index.html (accessed on 12 January 2023).
33. Overview of Shanghai. Available online: https://www.shanghai.gov.cn/nw2318/index.html (accessed on 12 January 2023).
34. Yang, G.; Fu, Y.; Yan, M.; Zhang, J. Exploring the Distribution of Energy Consumption in a Northeast Chinese City Based on Local Climate Zone Scheme: Shenyang City as a Case Study. *Energy Explor. Exploit.* **2020**, *38*, 2079–2094. [CrossRef]
35. Overview of Shenyang City. Available online: http://www.shenyang.gov.cn/wssy/scfm/csgk/ (accessed on 13 January 2023).
36. Overview of Xi'an City. Available online: https://www.xa.gov.cn/sq/csgk/zrdl/1.html (accessed on 13 January 2023).
37. Almorox, J.; Hontoria, C.J.E.C. Global Solar Radiation Estimation Using Sunshine Duration in Spain. *Energy Convers. Manag.* **2004**, *45*, 1529–1535. [CrossRef]
38. *CJJ/T 85—2017*; Standard for Classification of Urban Green Space. Ministry of Housing and Urban-Rural Development of the People's Republic of China; China Architecture and Building Press: Beijing, China, 2017.
39. Data Set of Built-Up Areas of Chinese Cities in 2020. Available online: https://www.scidb.cn/en/detail?dataSetId=5876ca6bf2064a9f9b8d4b092a7a7ba9&dataSetType=journal (accessed on 4 July 2023).
40. Jin, H.; Bao, G.; Chen, J.; Chopping, M.; Jin, E.; Mandakh, U.; Jiang, K.; Huang, X.; Bao, Y.; Vandansambuu, B. Modifying the Maximal Light-Use Efficiency for Enhancing Predictions of Vegetation Net Primary Productivity on the Mongolian Plateau. *Int. J. Remote Sens.* **2020**, *41*, 3740–3760. [CrossRef]
41. Ruimy, A.; Saugier, B.; Dedieu, G. Methodology for the Estimation of Terrestrial Net Primary Production from Remotely Sensed Data. *J. Geohys. Res. Atmos.* **1994**, *99*, 5263–5283. [CrossRef]
42. Field, C.B.; Randerson, J.T.; Malmström, C.M. Global Net Primary Production: Combining Ecology and Remote Sensing. *Remote Sens. Environ.* **1995**, *51*, 74–88. [CrossRef]
43. Zhu, W.; Pan, Y.; He, H.; Yu, D.; Hu, H. Simulation of Maximum Light Use Efficiency for Some Typical Vegetation Types in China. *Chin. Sci. Bull.* **2006**, *51*, 457–463. [CrossRef]
44. Liu, F.; Zeng, Y. Analysis of the Spatio-Temporal Variation of Vegetation Carbon Source/Sink in Qinghai Plateau from 2000–2015. *Acta Ecol. Sin.* **2021**, *41*, 5792–5803.
45. Pei, Z.; Zhou, C.; Ouyang, H.; Yang, W. A Carbon Budget of Alpine Steppe Area in the Tibetan Plateau. *Geogr. Res.* **2010**, *29*, 102–110.
46. Swetnam, T.L.; Lynch, A.M.; Falk, D.A.; Yool, S.R.; Guertin, D.P. Discriminating Disturbance from Natural Variation with LiDAR in Semi-Arid Forests in the Southwestern USA. *Ecosphere* **2015**, *6*, 1–22. [CrossRef]
47. Fallah, G.; Dadash, A. An Investigation on Thermal Patterns in Iran Based on Spatial Autocorrelation. *Theor. Appl. Climatol.* **2018**, *131*, 865–876. [CrossRef]
48. Li, D.; Wang, Z. The Characteristics of NPP of Terrestrial Vegetation in China Based on MOD17A3 Data. *Ecol. Environ. Sci.* **2018**, *27*, 397–405.
49. Turner, D.P.; Ritts, W.D.; Cohen, W.B.; Maeirsperger, T.K.; Gower, S.T.; Kirschbaum, A.A.; Running, S.W.; Zhao, M.; Wofsy, S.C.; Dunn, A.L.; et al. Site-Level Evaluation of Satellite-Based Global Terrestrial Gross Primary Production and Net Primary Production Monitoring. *Glob. Change Biol.* **2005**, *11*, 666–684. [CrossRef]
50. Li, Z.; Cheng, X.; Han, H. Analyzing Land-Use Change Scenarios for Ecosystem Services and their Trade-Offs in the Ecological Conservation Area in Beijing, China. *Int. J. Environ. Res. Public. Health* **2020**, *17*, 8632. [CrossRef] [PubMed]
51. Zhang, M.; Kafy, A.A.; Ren, B.; Zhang, Y.; Tan, S.; Li, J. Application of the Optimal Parameter Geographic Detector Model in the Identification of Influencing Factors of Ecological Quality in Guangzhou, China. *Land* **2022**, *11*, 1303. [CrossRef]
52. Wu, Y.; Wu, Z. Quantitative Assessment of Human-Induced Impacts Based on Net Primary Productivity in Guangzhou, China. *Environ. Sci. Pollut. Res.* **2018**, *25*, 11384–11399. [CrossRef]
53. Zhan, J.; Zhang, F.; Chu, X.; Liu, W.; Zhang, Y. Ecosystem Services Assessment Based on Emergy Accounting in Chongming Island, Eastern China. *Ecol. Indic.* **2019**, *105*, 464–473. [CrossRef]
54. Eisfelder, C.; Kuenzer, C. Investigating Fourteen Years of Net Primary Productivity Based on Remote Sensing Data for China. In *Remote Sensing Time Series: Revealing Land Surface Dynamics*; Springer: Cham, Switzerland, 2015; pp. 269–288.
55. Chen, T.; Liu, M.; Hu, Y.; Lu, J.; Ma, J.; Sun, F.; Gong, J. Land Use and Net Primary Productivity Changes in Shenyang Metropolitan Area. *Acta Ecol. Sin.* **2015**, *35*, 8231–8240.
56. Liang, C.; Su, H.; Zhang, Y.; Wang, J. Spatial-Temporal Changes and Influencing Factors Of Net Primary Productivity of Guanzhong Plain City Cluster from 2000 to 2019. *Res. Soil Water Conserv.* **2023**, *30*, 293–300.
57. Zhu, M. Study on the Carbon Fixation Evaluation of the Green-Land System in the Xi 'an Chanba Eco-Region. Master's Thesis, Xi'an University of Architecture and Technology, Xi'an, China, 2020.
58. Goncharova, O.; Matyshak, G.; Udovenko, M.; Semenyuk, O.; Epstein, H.; Bobrik, A. Temporal Dynamics, Drivers, and Components of Soil Respiration in Urban Forest Ecosystems. *Catena* **2020**, *185*, 104299. [CrossRef]
59. Huang, L.; Zhang, Y.; Deng, Y.; Lin, L.; Liu, X.; Xiao, R. The Carbon Footprint Accounting and Assessment of Urban Green Space—Taking Guangzhou as an Example. *For. Resour. Manag.* **2017**, *2*, 65–73.

60. Yang, F.; Wang, H. A Review of the Usability of Research Results on Carbon Sink and Carbon Emission in Urban Green Space from the Perspective of Planning and Design Practice. *Landsc. Archit.* **2023**, *40*, 71–78.

61. Guo, Z.; Zhang, Z.; Wu, X.; Wang, J.; Zhang, P.; Ma, D.; Liu, Y. Building Shading Affects the Ecosystem Service of Urban Green Spaces: Carbon Capture in Street Canyons. *Ecol. Model.* **2020**, *431*, 109178. [CrossRef]

62. Lindén, L.; Riikonen, A.; Setälä, H.; Yli-Pelkonen, V. Quantifying Carbon Stocks in Urban Parks Under Cold Climate Conditions. *Urban For. Urban Green.* **2020**, *49*, 126633. [CrossRef]